Applied and Computational Mechanics 7 (2013) 65–76

Application of patch test in meshless analysis of continuously non-homogeneous piezoelectric circular plate

P. Staňák[a,*], V. Sládek[a], J. Sládek[a], S. Krahulec[a], L. Sátor[a]

[a] *Institute of Construction and Architecture, Slovak Academy of Sciences, Dúbravská cesta 9, 845 03 Bratislava, Slovakia*

Received 12 December 2012; received in revised form 6 March 2013

Abstract

Proposed paper presents application of the patch test for meshless analysis of piezoelectric circular plate with functionally graded material properties. Functionally graded materials (FGM) are the special class of composite materials with continuous variation of volume fraction of constituents in predominant direction. Patch test analysis is an important tool in numerical methods for addressing the convergence. Meshless local Petrov-Galerkin (MLPG) method together with moving least-squares (MLS) approximation scheme is applied in the analysis. No finite elements are required for approximation or integration of unknown quantities. Circular plate is considered as a 3-D axisymmetric piezoelectric solid. Considering the axial symmetry, the problem is reduced to a 2-dimensinal one. Displacement and electric potential fields are prescribed on the outer boundaries in order to reach the state of constant stress field inside the considered plate as required by the patch test and the governing equations. Values of prescribed mechanical and electrical fields must be determined in order to comply with applied FGM gradation rule. Convergence study is performed to assess the considered meshless approach and several conclusions are finally presented.

Keywords: patch test, meshless method, functionally graded materials, MLS approximation

1. Introduction

Piezoelectric materials have found wide range of applications as sensors and actuators in variety of advanced engineering systems and structures. Structures which incorporate piezoelectric or another smart material are usually called adaptive structures. In this way various possibilities of vibration suppression, structural health monitoring and shape control are available [1, 8]. Smart materials are characterized by ability of converting energy form one form into another by response to an external impulse, for piezoelectric materials it is conversion of mechanical energy to electrical one and opposite. Many piezoelectric structures have plate-like shapes. Such devices can be found in acoustic ultrasound resonators or certain types of accelerometers and sensors. Active piezoelectric elements laminated into multilayer composite plates can significantly improve its structural properties [7]. Important investigations in the field of piezoelectric plates were first introduced by Tiersten [19].

Recently also the functionally graded materials (FGMs) [18] have been widely applied in engineering applications because of their excellent properties. FGMs are multi-component composite materials in which the volume fraction of the material constituents is continuously varying in a predominant direction. This feature can be used to tune the selected properties into desired value. Originally these materials have been introduced to benefit from the ideal

*Corresponding author. Tel.: +421 259 309 295, e-mail: peter.stanak@savba.sk.

performance of its constituents, e.g. for thermal shielding applications where high thermal resistance of the ceramics on the one side and mechanical strength of metals on the other side is utilized. Similarly also piezoelectric parameters can be enhanced if various piezoelectric ceramic materials are combined.

Design of structures incorporating piezoelectric and functionally graded materials requires advanced computational techniques for analysis of these materials under various operational conditions. Development of new computational methods for solving such complex problems requires tools for checking the quality of computed results. The patch test can be considered as one of such numerical procedures to address the convergence of the applied method. Convergence, in sense of numerical computing, describes how the results, under specific conditions, approach the exact solution. The patch test was developed primary for the finite element method (FEM) however can be used also to other computational methods.

The test, in its original form, is based on selecting a patch (group) of finite elements and imposing upon it nodal displacements corresponding to any state of constant strain. Rigid body condition is also satisfied by the patch test if displacement field corresponding to zero strain is imposed. If the FE model passes the patch test, one can expect that the solution will converge to exact values as the mesh is refined. The patch test was first introduced by Irons and Razzaque [8] to examine the soundness of a nonconforming plate element. In this original form, the patch test was primarily a test for polynomial completeness, i.e. the ability to reproduce exactly a polynomial of order k [4].

Even though the finite element method has encountered wide acceptance and success on commercial market, it possess some drawbacks such as locking of elements, stress discontinuity across elements or costly remeshing in large problems with moving boundaries. The meshless methods, an attractive option to solve these drawbacks were developed in the last decade. Among many meshless or meshfree methods available the meshless local Petrov-Galerkin (MLPG) method [2, 3] has received considerable scientific attention. Focusing on nodes instead of finite elements have certain advantages. High computational demands of remeshing in large scale problems or possible shear locking of elements appearing in the FEM can be efficiently eliminated. MLPG was recently applied to broad field of engineering problems including laminated plates [12], rectangular piezoelectric plates [13] or 3-D axisymmetric piezoelectric solids [10]. Thermal bending of plates with functionally graded material properties analyzed by MLPG was presented in [11]. Recently, FGM circular plates were also analyzed [14] and solutions for composite circular plates with piezoelectric layers were presented [16, 17]. The patch test of the MLPG solution was performed for the Laplace equation on the square domain in [3] with successful results. Sladek et al. [15] used the patch test to examine the accuracy of various meshless interpolations in non-homogeneous media. If the MLPG method recovers the prescribed exact solution at all interior nodes, then the method passes the patch test [2].

Presented paper is adressing the modified patch test for the functionally graded piezoelectric circular plate analyzed by the MLPG method. The circular plate can be considered as a 3-D axisymmetric body with axis of symmetry passing through the center of the plate coinciding with vertical z-axis. With use of cylindrical coordinates the original 3-D axisymmetric problem can be reduced to 2-D problem located on the cross-section of the plate as shown in Fig. 1.

The coupled electro-mechanical fields are described by constitutive relations and governing partial differential equations (PDEs). Nodal points are spread on the analyzed domain without any restrictions. Small local circular subdomain is introduced around each nodal point. Local integral equations (LIEs) constructed from governing PDEs are defined over these circular sub-

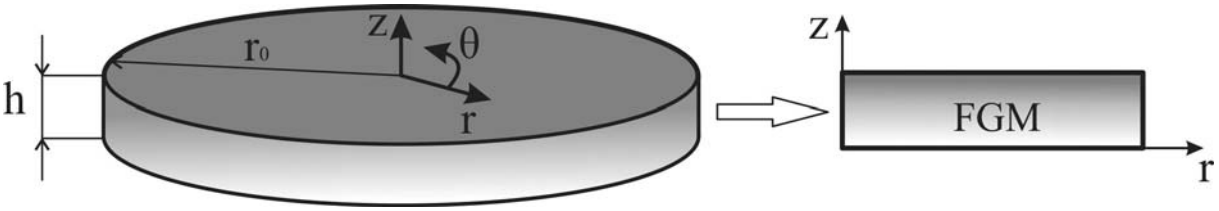

Fig. 1. Geometry of the circular plate: a) original 3-D problem, b) assumed 2-D geometry

domains. For a simple shape of subdomains e. g. circles, numerical integration of LIEs can be easily carried out. Moving Least-Squares (MLS) approximation scheme [2,6] is used to approximate the spatial variations of electric and mechanical fields. Since position of nodal points is not restricted by any finite elements, random distribution of nodes is possible, in general. There is also no restriction on the shape of analysed domain, however one have to keep in mind that sufficient ammount of nodes must be applied to adequately capture the geometry and mantain an accurate approximation of nodal quantities.

An exponential variation of material properties is assumed for the FGM plate. In order to obtain the state of constant stress satisfying the governing equations the axial displacement and electric potential must be specified on the outer boundaries in a form that comply well with prescribed FGM gradation. Compared to homogeneous materials the non-constant strain field is present, thus the original conditions of the patch test must be modified. The essential boundary conditions and prescribed mechanical and electrical fields are satisfied by the collocation of MLS approximation expressions on boundary nodes.Convergence study for increasing number of nodal points is finally conducted and results are discussed.

2. Governing equations

Piezoelectric materials are characterized by mutual coupling of elastic field and electric field. Quasi-static approximation of electric field is assumed, thus mechanical and electrical forces are balanced at any time instant. Governing equations for general piezoelectric body under static loading are given by the elastostatic equations and the first Maxwell's equation for the vector of electric displacements as

$$\sigma_{ij,j}(\mathbf{x}) + X_i(\mathbf{x}) = 0, \tag{1}$$

$$D_{i,i}(\mathbf{x}) - R(\mathbf{x}) = 0, \tag{2}$$

where σ_{ij}, D_i, X_i, R are stresses, electric displacements, vector of body forces and volume density of free charges, respectively. The linear constitutive equations for functionally graded piezoelectric material can be expressed as

$$\sigma_{ij}(\mathbf{x}) = C_{ijkl}(\mathbf{x})\varepsilon_{kl}(\mathbf{x}) - e_{kij}(\mathbf{x})E_k(\mathbf{x}), \tag{3}$$

$$D_i(\mathbf{x}) = e_{ikl}(\mathbf{x})\varepsilon_{kl}(\mathbf{x}) + h_{ik}(\mathbf{x})E_k(\mathbf{x}), \tag{4}$$

where $C_{ijkl}(\mathbf{x})$, $e_{kij}(\mathbf{x})$, $h_{ik}(\mathbf{x})$ represent spatially dependent elastic, piezoelectric and dielectric material coefficients, respectively. The strain tensor ε_{ij} and electric field vector E_k are related to elastic displacements u_i and electric potential ψ by

$$\varepsilon_{ij} = \frac{1}{2}(u_{i,j} + u_{j,i}), \tag{5}$$

$$E_k = -\psi_{,k}. \tag{6}$$

Since the considered problem is assumed to be axisymmetric, it can be reduced to 2-D, if cylindrical coordinates $\mathbf{x} = [r, \theta, z]$ are used. All physical quantities are then independent of angular coordinate θ, thus $\mathbf{x}$ becomes $\mathbf{x} = [r, z]$. Finally, for the axisymmetric piezoelectric body we can rewrite the governing equations (1), (2) into the following cylindrical coordinate form

$$\sigma_{rr,r}(r,z) + \sigma_{rz,z}(r,z) + \frac{\sigma_{rr}(r,z) - \sigma_{\theta\theta}(r,z)}{r} = 0, \tag{7}$$

$$\sigma_{rz,r}(r,z) + \sigma_{zz,z}(r,z) + \frac{\sigma_{rz}(r,z)}{r} = 0, \tag{8}$$

$$D_{r,r}(r,z) + D_{z,z}(r,z) + \frac{D_r(r,z)}{r} = 0, \tag{9}$$

where volume density of body forces and volume density of free charges are vanishing. The constitutive equations (3), (4) are rewritten for orthotropic piezoelectric materials in cylindrical coordinates as

$$\sigma_{rr} = c_{11}\varepsilon_{rr} + c_{12}\varepsilon_{\theta\theta} + c_{13}\varepsilon_{zz} - e_{31}E_z, \tag{10}$$

$$\sigma_{\theta\theta} = c_{12}\varepsilon_{rr} + c_{11}\varepsilon_{\theta\theta} + c_{13}\varepsilon_{zz} - e_{31}E_z, \tag{11}$$

$$\sigma_{zz} = c_{13}\varepsilon_{rr} + c_{13}\varepsilon_{\theta\theta} + c_{33}\varepsilon_{zz} - e_{33}E_z, \tag{12}$$

$$\sigma_{rz} = c_{44}\varepsilon_{rz} - e_{15}E_r, \tag{13}$$

$$D_r = e_{15}\varepsilon_{rz} + h_{11}E_r, \tag{14}$$

$$D_z = e_{31}\varepsilon_{rr} + e_{31}\varepsilon_{\theta\theta} + e_{33}\varepsilon_{zz} + h_{33}E_z. \tag{15}$$

The strain tensor ε_{ij} is then related to elastic displacements u_i as

$$\varepsilon_{rr} = u_{r,r}, \qquad \varepsilon_{\theta\theta} = \frac{1}{r}u_r, \qquad \varepsilon_{zz} = u_{z,z}, \qquad \varepsilon_{rz} = u_{r,z} + u_{z,r}. \tag{16}$$

Note again that angular strain $\varepsilon_{\theta\theta}$ is nonzero and independent of angular coordinate.

Governing equations (7)–(9) must be followed by essential and/or natural boundary conditions that are assumed for elastic and electrical fields as

$$u_i(\mathbf{x},t) = \tilde{u}_i(\mathbf{x},t) \text{ on } \Gamma_u, \quad \sigma_{ij}n_j = \tilde{T}_i(\mathbf{x},t) \text{ on } \Gamma_t, \tag{17}$$

$$\psi(\mathbf{x},t) = \tilde{\psi}(\mathbf{x},t) \text{ on } \Gamma_p, \quad D_i n_i = \tilde{Q}(\mathbf{x},t) \text{ on } \Gamma_q, \tag{18}$$

where n_i is the unit outward normal vector, Γ_u, Γ_t, Γ_p, Γ_q are parts of the global boundary Γ with prescribed displacements $\tilde{u}_i$, tractions $\tilde{T}_i$, electric potential $\tilde{\psi}$ and surface density of electric induction field flux $\tilde{Q}$ (normal component of electric displacements), respectively.

3. Local integral equations

The MLPG method is based on the local weak form of the governing equations that is written over local subdomain Ω_s. The local subdomain is a small region taken for each node inside the global domain [2]. The local subdomains could be of any geometrical shape. In this paper the local subdomains posses circular shape — just for simplicity. The local weak forms of (5)–(7) can be then written as

$$\int_{\Omega_s} \sigma_{rr,r}(r,z)p^* \,\mathrm{d}\Omega + \int_{\Omega_s} \sigma_{rz,z}(r,z)p^* \,\mathrm{d}\Omega + \int_{\Omega_s} \frac{1}{r}\left[\sigma_{rr}(r,z) - \sigma_{\theta\theta}(r,z)\right] p^* \,\mathrm{d}\Omega = 0, \quad (19)$$

$$\int_{\Omega_s} \sigma_{rz,r}(r,z)q^* \,\mathrm{d}\Omega + \int_{\Omega_s} \sigma_{zz,z}(r,z)q^* \,\mathrm{d}\Omega + \int_{\Omega_s} \frac{1}{r}\sigma_{rz}(r,z)q^* \,\mathrm{d}\Omega = 0, \quad (20)$$

$$\int_{\Omega_s} D_{r,r}(r,z)w^* \,\mathrm{d}\Omega + \int_{\Omega_s} D_{z,z}(r,z)w^* \,\mathrm{d}\Omega + \int_{\Omega_s} \frac{1}{r}D_r(r,z)w^* \,\mathrm{d}\Omega = 0, \quad (21)$$

where $p^*(\mathbf{x})$, $q^*(\mathbf{x})$, $w^*(\mathbf{x})$ are arbitrary test functions. The Heaviside unit step functions are chosen as test functions for the present problem in the same way as in [17]. The local weak forms are the starting point for deriving local integral equations (LIEs) with the use of Gauss divergence theorem

$$\int_{\partial\Omega_s} \sigma_{rr}(r,z)n_r \,\mathrm{d}\Gamma + \int_{\partial\Omega_s} \sigma_{rz}(r,z)n_z \,\mathrm{d}\Gamma + \int_{\Omega_s} \frac{1}{r}\left[\sigma_{rr}(r,z) - \sigma_{\theta\theta}(r,z)\right] \,\mathrm{d}\Omega = 0, \quad (22)$$

$$\int_{\partial\Omega_s} \sigma_{rz}(r,z)n_r \,\mathrm{d}\Gamma + \int_{\partial\Omega_s} \sigma_{zz}(r,z)n_z \,\mathrm{d}\Gamma + \int_{\Omega_s} \frac{1}{r}\sigma_{rz}(r,z) \,\mathrm{d}\Omega = 0, \quad (23)$$

$$\int_{\partial\Omega_s} D_r(r,z)n_r \,\mathrm{d}\Gamma + \int_{\partial\Omega_s} D_z(r,z)n_z \,\mathrm{d}\Gamma + \int_{\Omega_s} \frac{1}{r}D_r(r,z) \,\mathrm{d}\Omega = 0, \quad (24)$$

where $\partial\Omega_s$ represents the boundary of the local subdomain Ω_s and n_r, n_z are the unit outward normal vectors.

3.1. Meshless discretization

Traditional mesh-based approaches use mesh of finite elements to discretize the solution domain, however in the MLPG method the solution domain is discretized solely using nodal points distributed without any restrictions in mutual position. Special techniques are required to approximate unknown quantities in terms of nodal values only. The moving least-squares (MLS) approximation is used in this paper for the approximation of displacements u_r, u_z and electric potential field ψ as

$$u_r(r,z) = \sum_{i=1}^{n} \phi^i(r,z)\hat{u}_r^i, \quad (25)$$

$$u_z(r,z) = \sum_{i=1}^{n} \phi^i(r,z)\hat{u}_z^i, \quad (26)$$

$$\psi(r,z) = \sum_{i=1}^{n} \phi^i(r,z)\hat{\psi}^i, \quad (27)$$

where the nodal values $\hat{u}_r^i$, $\hat{u}_z^i$, $\hat{\psi}^i$ are so called fictitious parameters for the displacements and electric potential, and $\phi^i(r,z)$ is called the MLS shape function associated with the node $i \in \{1,2,\ldots,n\}$ and n is the number of nodes whose support domains involve the evaluation point (r,z). As a weight function, the 4^{th} order spline-type function [2] is used, ensuring C^1 continuity in the analyzed domain. In the similar manner also the appropriate derivatives can be obtained with use of the shape function derivative as

$$u_{j,k}(r,z) = \sum_{i=1}^{n} \phi^i_{,k}(r,z)\hat{u}_j^i, \qquad \psi_{,k}(r,z) = \sum_{i=1}^{n} \phi^i_{,k}(r,z)\hat{\psi}^i, \quad (28)$$

where $\phi^i_{,k}(r,z)$ represents the MLS shape function derivative.

Applying the trial functions given by (25)–(27) for approximation of $u_r(r,z)$, $u_z(r,z)$, $\psi(r,z)$ and their derivatives in constitutive relations (10)–(15) and their subsequent insertion into local integral equations (22)–(24) is leading to the discretized local integral equations in the form

$$\sum_{i=1}^{n} \hat{u}_r^i \int_{\partial\Omega_s} \left[c_{11}(\mathbf{x}) n_r \phi^i_{,r}(r,z) + \frac{c_{12}(\mathbf{x})}{r} n_r \phi^i(r,z) + c_{44}(\mathbf{x}) n_z \phi^i_{,z}(r,z) \right] \mathrm{d}\Gamma +$$
$$\sum_{i=1}^{n} \hat{u}_r^i \int_{\Omega_s} \left[\frac{c_{11}(\mathbf{x})}{r} \phi^i_{,r}(r,z) + \frac{c_{12}(\mathbf{x})}{r^2} \phi^i(r,z) - \frac{c_{11}(\mathbf{x})}{r^2} \phi^i(r,z) - \frac{c_{12}(\mathbf{x})}{r} \phi^i_{,r}(r,z) \right] \mathrm{d}\Omega +$$
$$\sum_{i=1}^{n} \hat{u}_z^i \int_{\partial\Omega_s} \left[c_{13}(\mathbf{x}) n_r \phi^i_{,z}(r,z) + c_{44}(\mathbf{x}) n_z \phi^i_{,r}(r,z) \right] \mathrm{d}\Gamma + \quad (29)$$
$$\sum_{i=1}^{n} \hat{\psi}^i \int_{\partial\Omega_s} \left[e_{31}(\mathbf{x}) n_r \phi^i_{,z}(r,z) + e_{15}(\mathbf{x}) n_z \phi^i_{,r}(r,z) \right] \mathrm{d}\Gamma = 0,$$

$$\sum_{i=1}^{n} \hat{u}_r^i \int_{\partial\Omega_s} \left[c_{44}(\mathbf{x}) n_r \phi^i_{,z}(r,z) + \frac{c_{13}(\mathbf{x})}{r} n_z \phi^i(r,z) + c_{13}(\mathbf{x}) n_z \phi^i_{,r}(r,z) \right] \mathrm{d}\Gamma +$$
$$\sum_{i=1}^{n} \hat{u}_r^i \int_{\Omega_s} \frac{c_{44}(\mathbf{x})}{r} \phi^i_{,z}(r,z)\,\mathrm{d}\Omega + \sum_{i=1}^{n} \hat{u}_z^i \int_{\partial\Omega_s} \left[c_{33}(\mathbf{x}) n_z \phi^i_{,z}(r,z) + c_{44}(\mathbf{x}) n_r \phi^i_{,r}(r,z) \right] \mathrm{d}\Gamma +$$
$$\sum_{i=1}^{n} \hat{u}_z^i \int_{\Omega_s} \frac{c_{44}(\mathbf{x})}{r} \phi^i_{,r}(r,z)\,\mathrm{d}\Omega + \sum_{i=1}^{n} \hat{\psi}^i \int_{\Omega_s} \frac{e_{15}(\mathbf{x})}{r} \phi^i_{,r}(r,z)\,\mathrm{d}\Omega + \quad (30)$$
$$\sum_{i=1}^{n} \hat{\psi}^i \int_{\partial\Omega_s} \left[e_{15}(\mathbf{x}) n_r \phi^i_{,r}(r,z) + e_{33}(\mathbf{x}) n_z \phi^i_{,z}(r,z) \right] \mathrm{d}\Gamma = 0,$$

$$\sum_{i=1}^{n} \hat{u}_r^i \int_{\partial\Omega_s} \left[e_{15}(\mathbf{x}) n_r \phi^i_{,z}(r,z) + \frac{e_{31}(\mathbf{x})}{r} n_z \phi^i(r,z) + e_{31}(\mathbf{x}) n_z \phi^i_{,r}(r,z) \right] \mathrm{d}\Gamma +$$
$$\sum_{i=1}^{n} \hat{u}_r^i \int_{\Omega_s} \frac{e_{15}(\mathbf{x})}{r} \phi^i_{,z}(r,z)\,\mathrm{d}\Omega + \sum_{i=1}^{n} \hat{u}_z^i \int_{\partial\Omega_s} \left[e_{15}(\mathbf{x}) n_r \phi^i_{,r}(r,z) + e_{33}(\mathbf{x}) n_z \phi^i_{,z}(r,z) \right] \mathrm{d}\Gamma +$$
$$\sum_{i=1}^{n} \hat{u}_z^i \int_{\Omega_s} \frac{e_{15}(\mathbf{x})}{r} \phi^i_{,r}(r,z)\,\mathrm{d}\Omega - \sum_{i=1}^{n} \hat{\psi}^i \int_{\partial\Omega_s} \left[h_{11}(\mathbf{x}) n_r \phi^i_{,r}(r,z) + h_{33}(\mathbf{x}) n_z \phi^i_{,z}(r,z) \right] \mathrm{d}\Gamma - \quad (31)$$
$$\sum_{i=1}^{n} \hat{\psi}^i \int_{\Omega_s} \frac{h_{11}(\mathbf{x})}{r} \phi^i_{,r}(r,z)\,\mathrm{d}\Omega = 0.$$

4. The patch test

If the patch test is applied to a homogeneous piezoelectric material, the linear displacement and potential field specified on the outer boundary will result into constant mechanical strains and constant electric field vector and thus also the governing equations (1) and (2) will be satisfied. However in case of continuously non-homogeneous FGM material imposed linear mechanical and electrical fields will satisfy condition of constant strain, but governing equations will not be satisfied and some external load would be required to maintain equilibrium. This is the reason why the modified patch test that does not require constant strain field is applied in the present paper. Nonlinear displacement and electric potential field are applied resulting in non-constant strains; however equilibrium is maintained for the analyzed plate.

Properties of functionally graded materials can be specified during their manufacturing process according the specific requirements of the design application. In the problem considered here the exponential variation of material properties in z direction is specified as

$$P(z) = P^{(0)}\mathrm{e}^{\delta z/h}, \tag{32}$$

where P is graded material property, $P^{(0)}$ is material property at the bottom of the plate, h is the height of the plate and δ is a gradation constant. Change of the gradation constant is resulting to the change of graded material property along the thickness of the plate.

Considering the variation of material properties (27), the axial displacement u_z and electric potential ψ can be specified on the outer boundaries of the plate as

$$u_z = u_{z0} + A\mathrm{e}^{-\delta z/h}, \qquad \psi = \psi_0 + B\mathrm{e}^{-\delta z/h}, \tag{33}$$

where u_{z0}, ψ_0, A are arbitrarily chosen constants, while the constant B can be determined after inserting (33) into the governing equations with vanishing the radial displacement $u_r = 0$.

Then the constant B is specified as

$$B = -\frac{c_{13}^{(0)}}{e_{31}^{(0)}}A. \tag{34}$$

Applying the relations (32)–(34) in the constitutive equation (10) for the radial stress gives

$$\begin{aligned}\sigma_{rr} &= c_{11}^{(0)}\mathrm{e}^{\delta z/h}0 + c_{12}^{(0)}\mathrm{e}^{\delta z/h}\frac{0}{r} + c_{13}^{(0)}\mathrm{e}^{\delta z/h}\left(-\frac{A\delta}{h}\right)\mathrm{e}^{-\delta z/h} + e_{31}^{(0)}\mathrm{e}^{\delta z/h}\left(\frac{c_{13}^{(0)}}{e_{31}^{(0)}}\frac{A\delta}{h}\right)\mathrm{e}^{-\delta z/h} = \\ &= -c_{13}^{(0)}\left(\frac{A\delta}{h}\right) + c_{13}^{(0)}\left(\frac{A\delta}{h}\right) = 0.\end{aligned} \tag{35}$$

In the same way we obtain the expressions of remaining constitutive equations (11)–(15) as

$$\sigma_{\theta\theta} = \sigma_{rz} = D_r = 0, \tag{36}$$

$$\sigma_{zz} = \left(-c_{33}^{(0)} + e_{33}^{(0)}\frac{c_{13}^{(0)}}{e_{31}^{(0)}}\right)\frac{A\delta}{h} = \text{const.}, \tag{37}$$

$$D_z = -\left(e_{33}^{(0)} + h_{33}^{(0)}\frac{c_{13}^{(0)}}{e_{31}^{(0)}}\right)\frac{A\delta}{h} = \text{const.} \tag{38}$$

Recall that in homogeneous media, the constant values of the secondary fields (stresses and electric displacements) and the constant values of the gradients of the primary fields (elastic displacements and the electric potential) are obeyed simultaneously. Now in FGM case, the use of the exponential variation for the prescribed axial displacement field and electric potential field (33) leads to exponential (non-constant) variation of axial strain and axial electric field vector

$$E_z = -\psi_{,z} = \frac{c_{13}^{(0)}}{e_{31}^{(0)}}\frac{A\delta}{h}\mathrm{e}^{-\delta z/h}, \qquad \varepsilon_{zz} = u_{z,z} = -\frac{A\delta}{h}\mathrm{e}^{-\delta z/h}. \tag{39}$$

This clearly denies the constant strain conditions. Nevertheless, the stresses as well as electric displacements are constant like in the case of patch test for homogeneous media. Moreover, the

considered fields represent the exact solution of the governing equations and can be employed in the patch test involving FGM.

The patch test is suitable for testing new computational methods because it directly offers an "exact" benchmark solution that can be utilized for the error estimation and convergence analysis. Equivalently the expression (33) can be considered as the exact solution to the plate subjected to applied tension

$$\tilde{T}_z(z=0) = \left(c_{33}^{(0)} - e_{33}^{(0)} \frac{c_{13}^{(0)}}{e_{31}^{(0)}} \right) \frac{A\delta}{h}, \tag{40}$$

$$\tilde{T}_z(z=h) = \left(-c_{33}^{(0)} + e_{33}^{(0)} \frac{c_{13}^{(0)}}{e_{31}^{(0)}} \right) \frac{A\delta}{h}, \tag{41}$$

$$\tilde{T}_r(r,z) = 0 \tag{42}$$

and prescribed potential field on the outer boundary

$$\psi(r,z) = \psi_o - \frac{c_{13}^{(0)}}{e_{31}^{(0)}} A \mathrm{e}^{-\delta z/h}. \tag{43}$$

In the MLPG solution, the collocation approach can be used to impose essential boundary conditions directly using the MLS approximations (25)–(27) for primary field variables directly. In the present paper these approximations are applied to specify the expression (33) on the boundary nodes.

5. Numerical example

The patch test is performed on the circular plate with radius $r_0 = 0.3$ m and thickness $h = 0.03$ m. PZT-4 piezoelectric material is considered as bottom material with properties taken from [17]. The considered rectangular geometry is discretized with nodal points only and no restrictions are set for the mutual position of nodes. Vanishing radial displacement and exponentially varying axial displacement is prescribed on the boundary nodes according to (33). The input constants are chosen as $u_{z0} = 0.03$ m, $\psi_0 = 5 \times 10^7$ V, $A = 0.01$ together with grading exponent $\delta = 0.693\,1$. Using this exponent is leading to material properties increased two times at the top of the plate, since according to (32) one gets

$$P(z=h) = P^{(0)} \mathrm{e}^{0.693\,1 \frac{h}{h}} = 2P^{(0)}. \tag{44}$$

Five nodal distributions were selected as 3×3, 5×5, 9×5, 11×7 and 15×7 corresponding to total 9, 25, 45, 77 and 105 nodes, respectively. For each nodal distribution the radius of support domain is chosen to cover all nodal points in order to avoid the sensitivity of the model to this parameter. The radius of support domain [2] is an important parameter for MLS approximation. It determines the number of nodes n that are used for approximation of unknown quantities in (25)–(28).

Numerical results for the axial displacement field $u_z(r,z)$ and electric potential field $\psi(r,z)$ are shown in Fig. 2 for the case with 11×7 nodal distribution. According to (35)–(37), the resulting radial stress and shear stress must vanish while axial stress should be constant. Results for these stresses evaluated at nodes located in the middle of the plate shown in Fig. 3 confirm this statement.

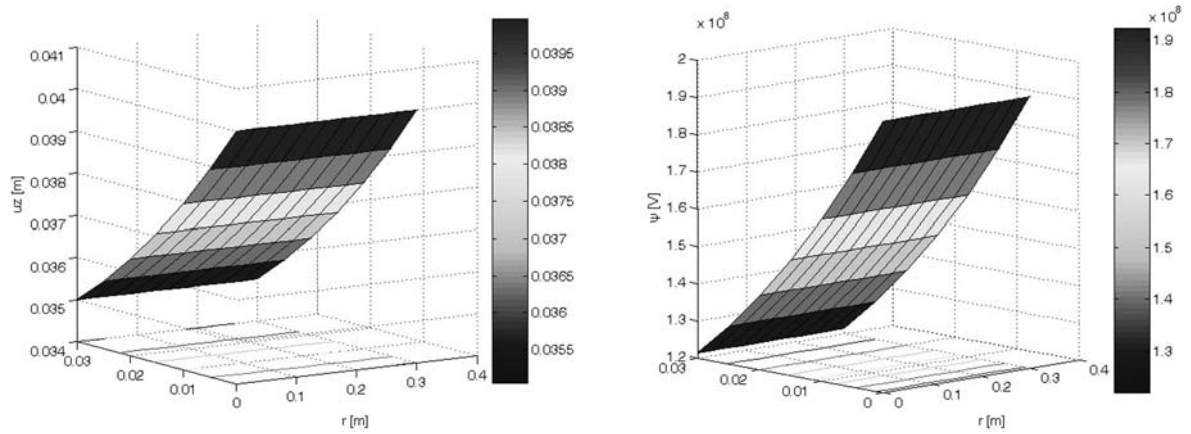

Fig. 2. Resulting axial displacement (left) and electric potential distribution (right)

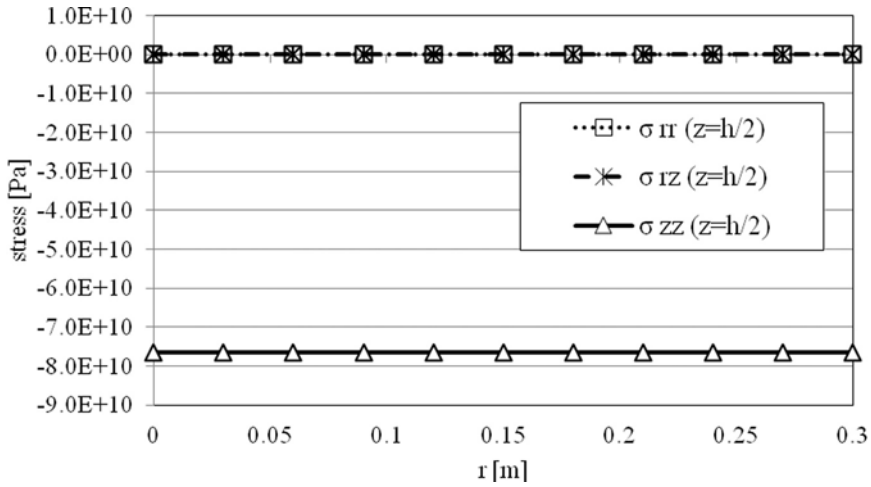

Fig. 3. Stress distribution taken at the middle of the plate ($z = h/2$)

Using the exact benchmark solution, one can compute relative errors of the numerical analysis. Relative errors are computed for axial displacements. The relative error for every node is specified in percentage as

$$e = 100\frac{|u_z^{num} - u_z^{exact}|}{|u_z^{exact}|}\ [\%], \tag{45}$$

where u_z^{num} represents computed value of axial displacement and u_z^{exact} represents "exact" solution as obtained by straightforward use of (33). Fig. 4 shows the distribution of relative error for 11×7 nodal distribution.

As can be seen in Fig. 4, relative error is much higher for the interior nodes compared to nodes on the boundary. The axial displacement on the boundary nodes is specified by the MLS approximation of (33) while for the interior nodes the results are obtained from the discretized LIE (30). The numerical integration of domain integrals in LIEs is probably causing the errors. Spline-type weight functions used in MLS approximation may generate complicated shape over the local subdomain Ω_s, which may be difficult to integrate. Breitkopf et al. [5] proposed custom integration scheme to integrate MLS shape functions correctly. However in the present paper, the standard Gauss integration scheme is chosen, since the error is in the acceptable level.

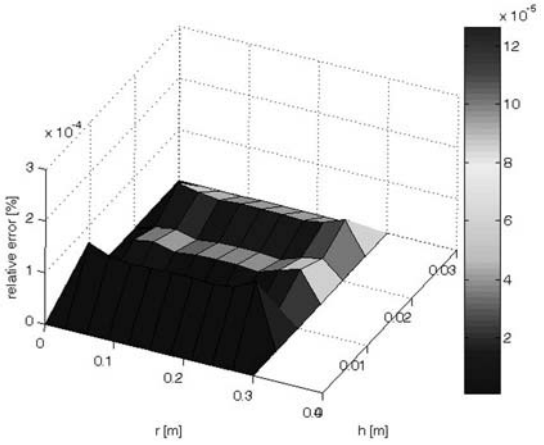

Fig. 4. Relative nodal error distribution over discretized plate

It may be convenient to specify other type of error estimation that would tackle the error of the numerical solution from the global viewpoint. Averaged percentage error [15] was introduced for this reason as

$$AE = 100\frac{\|u_z^{num} - u_z^{exact}\|}{\|u_z^{exact}\|}\ [\%], \tag{46}$$

where the norm is given as $\|*\| = \left(\sum_{a=1}^{N_t}\left[*\left(\mathbf{x}^a\right)\right]^2\right)^{\frac{1}{2}}$ and N_t is the total number of nodes used in the analysis. Using this error estimate the convergence of the method for varying nodal densities can be determined as shown in Fig. 5. Both the axial displacement and the electric potential convergence are analyzed. Results show that the axial displacement is reaching better accuracy than the electric potential; however the convergence rate for both quantities is almost the same. The convergence curve for the axial displacement also indicates the increase of accuracy with increasing the number of nodes in z-axis direction, since the material gradation is in the same direction.

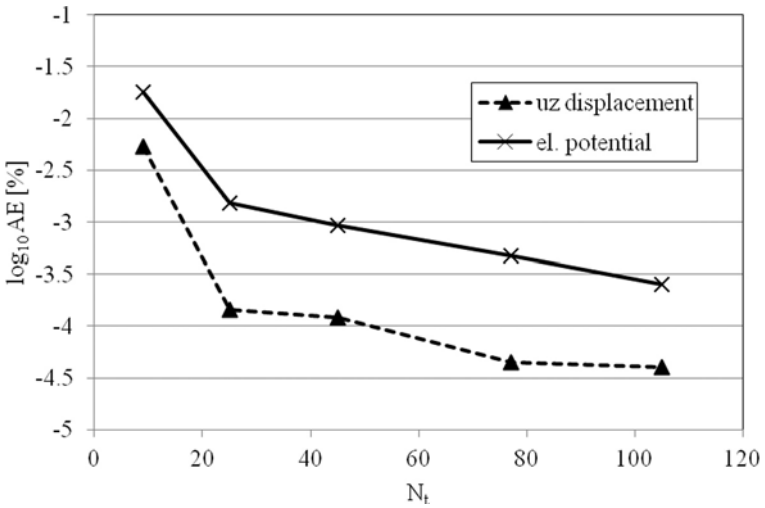

Fig. 5. Averaged relative error distribution and convergence rate

6. Conclusion

The patch test is an important tool used in development of new numerical computational techniques. In the present paper the patch test is used to examine convergence of meshless solution for functionally graded piezoelectric circular plate. The employed meshless MLPG method is a truly meshless method since no elements are required neither for approximation nor for integration of unknowns. The MLS approximation is applied to approximation of unknown elastic as well as electric quantities.

The patch test analysis of material with constant material properties requires constant strain field (produced by applied linear displacement field) to maintain the equilibrium, this is however not the case for continuously non-homogeneous material. Non-linear distribution of displacement and electrical fields were derived as the exact solution of the governing equations involving the exponential material gradation rule. The numerical example showed that the developed formulation passed the patch test with positive convergence for increased number of nodes.

The patch test was presented as a simple tool for verification of new computer codes since the data are easy to prepare and the exact benchmark results are instantly applicable for determination of accuracy and convergence of numerical results.

Acknowledgements

The present paper has been supported by the Slovak Science and Technology Assistance Agency through the grant registered under number APVV-0014-10. The support is gratefully acknowledged.

References

[1] Adachi, A., Kitamura, Y., Iwatsubo, T., Integrated design of piezoelectric damping system for flexible structure, Applied Acoustics 65 (2004) 293–310.

[2] Atluri, S. N., The Meshless Method (MLPG) For Domain & BIE Discretizations, Tech Science Press, Forsyth, GA, 2004.

[3] Atluri, S. N., Zhu, T., A new meshless local Petrov-Galerkin (MLPG) approach in computational mechanics, Computational Mechanics 22 (1998) 117–127.

[4] Belytschko, T., Liu, W. K., Moran, B., Nonlinear Finite Elements for Continua and Structures, John Willey & Sons, Chichester, England, 2000.

[5] Breitkopf, P., Rassineux, A.,Villon, P., Custom integration scheme for patch test in MLS meshfree methods, Computational Fluid and Solid Mechanics 2003 (K. J. Bathe (Ed.)), Elsevier Ltd, 2003, pp. 1 876–1 879.

[6] Lancaster, P., Salkauskas, T., Surfaces generated by moving least square methods, Mathematics of Computation 37 (1981) 141–158.

[7] Liew, K. M., Lim, H. K., Tan, M. J., He, X. Q., Analysis of composite beams and plates with piezoelectric patches using the element-free Galerkin method, Computational Mechanics 29 (2002) 486–497.

[8] Irons, B. M., Razzaque, A., Experience with the patch test for convergence of finite element method. In: The Mathematics of Finite Elements with Application to Partial Differential Equations (Aziz, A. R. (Ed.)), Academic Pres USA, 1972, p. 557–587.

[9] Semedo Garção, J. E., Mota Soares, C. M., Mota Soares, C. A., Reddy, J. N., Analysis of laminated adaptive plate structures using layerwise finite elements, Computers and Structures 82 (2004) 1 939–1 959.

[10] Sladek, J., Sladek, V., Solek, P., Saez, A., Dynamic 3D axisymmetric problems in continuously nonhomogeneous piezoelectric solids, International Journal of Solids and Structures 45 (2008) 4 523–4 542.

[11] Sladek, J., Sladek, V., Solek, P., Wen, P. H., Thermal Bending of Reissner-Mindlin Plates by the MLPG, CMES – Computer Modeling in Engineering & Sciences 28 (2008) 57–76.

[12] Sladek, J., Sladek, V., Stanak, P., Zhang, Ch., Meshless Local Petrov-Galerkin (MLPG) Method for Laminate Plates under Dynamic Loading, CMC – Computers, Materials & Continua 15 (2010) 1–26.

[13] Sladek, J., Sladek, V., Stanak, P., Pan, E., The MLPG for bending of electroelastic plates, CMES – Computer Modeling in Engineering & Sciences 64 (2010) 267–298.

[14] Sladek, J., Sladek, V., Stanak, P., Zhang, Ch., Wunshe, M., Bending of circular piezoelectric plates with functionally graded material properties. Proceedings Third International Symposium on Computational Mechanics in conjunction with Second Symp. on Comp. Structural Enginering. ((Ed) Yeong-Bin Yang, Liang-Jeng Leu, Chuin-Shan David Chen), Taipei, National Taiwan University Press, 2011, pp. 42–43.

[15] Sladek, V., Sladek, J., Tanaka, M., Local Integral Equations and two Meshless Polynomial Interpolations with Application to Potential Problems in Non-homogeneous Media, CMES – Computer Modeling in Engineering & Sciences 7 (2005) 69–83.

[16] Stanak, P., Sladek, J., Sladek, V., Krahulec, S., Bending of functionally graded circular plates with piezoelectric layer by the MLPG method. Proceedings of 18^{th} International conference Engineering Mechanics 2012 (J. Naprstek, C. Fisher (Eds.)), Svratka Czech Republic. ITAM CAS Prague, 2012.

[17] Stanak, P., Sladek, J., Sladek, V., Krahulec, S., Composite circular plate analyzed as a 3-D axisymmetric piezoelectric solid, Building Research Journal 59, (2011) 125–140.

[18] Suresh, S., Mortensen, A., Fundamentals of Functionally Graded Materials, Institute of Materials, London, 1998.

[19] Tiersten, H. F., Linear piezoelectric plate vibrations, Plenum Press, New York, 1969.